Analytical Modeling and Numerical Simulation of Capacitive Silicon Bulk Acoustic Resonators

G. Casinovi, X. Gao and F. Ayazi

IEEE International Conference on Micro Electro Mechanical Systems
pp. 935–938, January 2009

Abstract

This paper introduces two newly developed models of capacitive silicon bulk acoustic resonators (SiBARs). The first model is analytical and is obtained from an approximate solution of the linear elastodynamics equations for the SiBAR geometry. The second is numerical and is based on finite-element, multi-physics simulation of both acoustic wave propagation in the resonator and electromechanical transduction in the capacitive gaps of the device. This latter model makes it possible to compute SiBAR performance parameters that cannot be obtained from the analytical model, e.g. the relationship between transduction area and insertion loss. Comparisons with measurements taken on a set of silicon resonators fabricated using electron-beam lithography show that both models can predict the resonant frequencies of SiBARs with a relative error smaller than 1%.

Copyright Notice

This material is presented to ensure timely dissemination of scholarly and technical work. Copyright and all rights therein are retained by authors or by other copyright holders. All persons copying this information are expected to adhere to the terms and constraints invoked by each author's copyright. In most cases, these works may not be reposted without the explicit permission of the copyright holder.

ANALYTICAL MODELING AND NUMERICAL SIMULATION OF CAPACITIVE SILICON BULK ACOUSTIC RESONATORS

G. Casinovi, X. Gao, and F. Ayazi
School of Electrical and Computer Engineering
Georgia Institute of Technology, Atlanta, Georgia, USA

ABSTRACT

This paper introduces two newly developed models of capacitive silicon bulk acoustic resonators (SiBARs). The first model is analytical and is obtained from an approximate solution of the linear elastodynamics equations for the SiBAR geometry. The second is numerical and is based on finite-element, multi-physics simulation of both acoustic wave propagation in the resonator and electromechanical transduction in the capacitive gaps of the device. This latter model makes it possible to compute SiBAR performance parameters that cannot be obtained from the analytical model, e.g. the relationship between transduction area and insertion loss. Comparisons with measurements taken on a set of silicon resonators fabricated using electron-beam lithography show that both models can predict the resonant frequencies of SiBARs with a relative error smaller than 1%.

INTRODUCTION

Much research activity in recent years has been directed at the development of bulk acoustic resonators that are compatible with standard integrated circuit technologies. In this respect, capacitive resonators [1–3] offer a particularly attractive option, since they can be made entirely of materials that are used routinely in IC fabrication processes, resulting in significant advantages in terms of ease of integration and cost savings.

Disk resonators were among the first examples of devices of this type [1], but more recently width-extensional-mode resonators based on an alternative, rectangular-bar geometry were demonstrated [2], [3], which are referred to as silicon bulk acoustic resonators, or SiBARs. The basic structure of a SiBAR is schematically shown in Figure 1: the resonating bar element is placed between two electrodes, supported by two thin tethers. A DC polarization voltage applied between the resonator and the electrodes generates an electrostatic field in the capacitive gaps. When an AC voltage is applied to the drive electrode, the electrostatic force applied to the corresponding face of the resonator induces an acoustic wave that propagates through the bar.

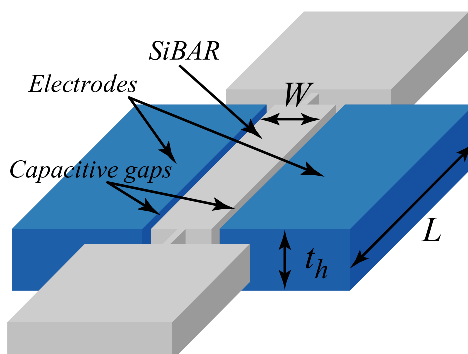

Figure 1: Structure of a SiBAR.

Small changes in the size of the capacitive gap on the other side of the device induce a voltage on the sense electrode, whose amplitude peaks near the mechanical resonant frequencies of the bar.

SiBARs offer several potential advantages over their disk-shaped counterparts, the most important of which is that the electrostatic transduction area can be increased without changing the main frequency-setting dimension, resulting in significantly lower motional resistance while maintaining high Q values [3].

While the behavior of SiBARs is well understood in broad, qualitative terms, a major obstacle to the design of high performance devices is a lack of sufficiently accurate analytical or numerical models. For example, to the authors' best knowledge there is currently no quantitative analysis of how exactly the dimensions of a SiBAR affect its insertion loss. Even the computation of the resonant frequencies is based on approximate formulae that, as will be shown in this paper, can be quite inaccurate, especially in the case of an anisotropic material such as single-crystal silicon.

This paper presents two newly developed SiBAR models, one analytical and the other numerical, that are significantly more accurate than currently available models. The analytical model is obtained from an approximate solution to the linear elastodynamics equations that satisfies the boundary conditions imposed by the SiBAR geometry. The second model is based on numerical multi-physics simulations of the device, performed in ANSYS. Comparisons with measurements taken on a set of devices fabricated using electron-beam lithography show that both models can predict the resonant frequencies of SiBARs of varying dimensions with a relative error of less than 1%.

ANALYTICAL MODEL

This section presents an analysis of acoustic wave propagation in a SiBAR, modeled as a bar of rectangular cross-section and made of a single, homogeneous, orthotropic material. The objective of this analysis is to obtain a quantitative model of the mechanical behavior of the resonator, which can then be used to compute the values of the resonant frequencies based on the resonator's dimensions and material properties.

From a mathematical point of view, an acoustic wave propagating through the resonator is represented by a vector $\mathbf{u} = [u_x, u_y, u_z]^T$, describing the displacement of a generic point in the device with respect to its position in the undeformed structure. In the analysis that follows, the x axis corresponds to the direction of the resonator's length (L), the y axis to the direction of its thickness (t_h), and the z axis to the direction of its width (W).

To simplify the analysis, the resonator length will be assumed to be infinite. Numerical simulation results and experimental measurements, presented later in this paper, show that this assumption does not result in a significant

978-1-4244-2978-3/09/$25.00 ©2009 IEEE

loss of accuracy, provided that the resonator's length is sufficiently large compared to the two other dimensions.

Symmetry considerations following from this assumption dictate that the solutions of interest are those that are independent of x and have no displacement component in the x direction (i.e. $u_x = 0$). Limiting the analysis to sinusoidal steady-state, such solutions can be expressed as

$$\mathbf{u}(y,z,t) = \begin{bmatrix} u_{y0} \\ u_{z0} \end{bmatrix} e^{j(\omega t - k_y y - k_z z)} \tag{1}$$

The expression above is a solution of the linear elastodynamics equations if and only if the following equation — generally known as the Christoffel equation [4] — is satisfied

$$\begin{bmatrix} c_{22}k_y^2 + c_{44}k_z^2 - \rho\omega^2 & (c_{23}+c_{44})k_y k_z \\ (c_{23}+c_{44})k_y k_z & c_{44}k_y^2 + c_{33}k_z^2 - \rho\omega^2 \end{bmatrix} \begin{bmatrix} u_{y0} \\ u_{z0} \end{bmatrix} = 0 \tag{2}$$

where ρ is the resonator mass density, and c_{22}, c_{23}, c_{33} and c_{44} are stiffness matrix coefficients.

Equation (2) has non-trivial solutions if and only if the determinant of the coefficient matrix is equal to zero, which, after some algebraic manipulation, leads to the following equation

$$\begin{aligned} & \rho^2 v^4 - (c_{33}+c_{44})\rho v^2 + c_{33}c_{44} \\ & + [c_{44}^2 + c_{22}c_{33} - (c_{23}+c_{44})^2 - \rho(c_{22}+c_{44})v^2]\zeta \\ & + c_{22}c_{44}\zeta^2 = 0 \end{aligned} \tag{3}$$

where $\zeta = (k_y/k_z)^2$ and $v = \omega/k_z$. For a given value of v, there are in general two solutions to (3), regarded as an equation in ζ, hence four values of the ratio k_y/k_z for which (2) has non-trivial solutions.

It is readily observed that the constant term in (3) — that is, the term that is independent of ζ — can also be written as $(\rho v^2 - c_{33})(\rho v^2 - c_{44})$. Let $v_u = \sqrt{c_{33}/\rho}$ and $v_l = \sqrt{c_{44}/\rho}$; note that $v_l \le v_u$ because $c_{44} \le c_{33}$. Consequently, if $v_l \le v \le v_u$ the constant term in (3) is negative, which means that in this case (3) has two real solutions, one positive and one negative. Letting $\zeta_1 = -\alpha^2$ and $\zeta_2 = \beta^2$, the possible values for k_y are $\pm j\alpha k_z$ and $\pm \beta k_z$. For each value of k_y, the corresponding values of u_{y0} and u_{z0} can be obtained from (2).

By superposition, a generic wave propagating through the resonator is a linear combination of four waves of the type given in (1), one for each possible value of k_y/k_z. This leads to the following expression for such wave

$$\begin{aligned} \mathbf{u}(y,z,t) = & A_0 \begin{bmatrix} j\alpha \sinh(\alpha k_z y) \\ u_{z0}\cosh(\alpha k_z y) \end{bmatrix} e^{j(\omega t - k_z z)} \\ & + A_1 \begin{bmatrix} j u_{y1}\sin(\beta k_z y) \\ \beta\cos(\beta k_z y) \end{bmatrix} e^{j(\omega t - k_z z)} \end{aligned} \tag{4}$$

where

$$u_{z0} = \frac{\rho v^2 + c_{22}\alpha^2 - c_{44}}{c_{23}+c_{44}}$$

and

$$u_{y1} = \frac{c_{44}\beta^2 + c_{33} - \rho v^2}{c_{23}+c_{44}}$$

Finally, coefficients A_0 and A_1 in (4) must be chosen so that the wave satisfies traction-free boundary conditions on the top and bottom faces of the resonator, that is

$$\sigma_{xy} = \sigma_{yy} = \sigma_{yz} = 0, \qquad y = \pm t_h/2$$

where σ_{xy}, σ_{yy} and σ_{yz} are components of the stress tensor. After some algebraic manipulation, those conditions lead to a homogeneous system of two linear equations in the two unknowns A_0 and A_1, which can have non-trivial solutions only if the determinant of the coefficient matrix is equal to zero. Making the substitution $k_z = 2\pi/\lambda_z$, where λ_z is the wavelength in the z direction, the condition on the determinant yields the following equation

$$\begin{aligned} & (c_{22}\alpha^2 - c_{23}u_{z0})(u_{y1} - \beta^2)\cosh(\pi\alpha\xi)\sin(\pi\beta\xi) \\ & - \alpha\beta(1+u_{z0})(c_{22}u_{y1} - c_{23})\sinh(\pi\alpha\xi)\cos(\pi\beta\xi) \\ & = 0 \end{aligned} \tag{5}$$

where $\xi = t_h/\lambda_z$. For fixed α and β, this is an equation in ξ which has infinitely many solutions, because of the periodicity of the sine and cosine terms. The expression for $\mathbf{u}$ in (4) and the relation between v and ξ derived from (5) are valid only for $v_l \le v \le v_u$, but the procedure outlined above requires only minor modifications to handle other ranges of values for v, e.g. $v \ge v_u$.

Since α and β depend on v through (3), equations (3) and (5), taken together, define a relation between v and ξ. Since (5) has multiple solutions, this relation defines a function $v = v(\xi)$ that has multiple branches. To each point (ξ, v) that lies on a branch of this function there corresponds an acoustic wave that propagates across the resonator.

Figure 2 shows the graph of $v(\xi)$ for single-crystal silicon, when the x and z reference axes are aligned with the and $\langle 0\bar{1}1\rangle$ and $\langle 011\rangle$ crystallographic directions, and the y axis with the $\langle 100\rangle$ direction. Only the first four of infinitely many branches of $v(\xi)$, or dispersion curves, are

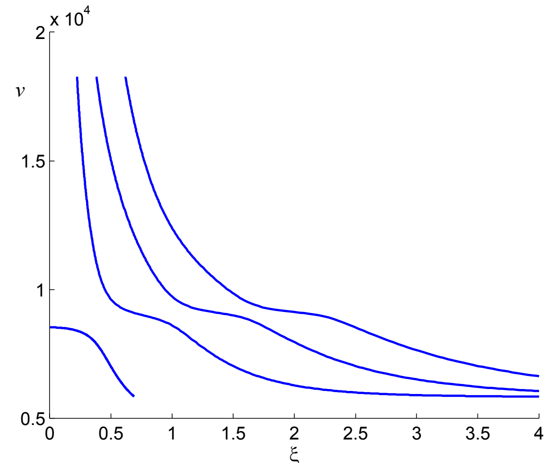

Figure 2: Propagation velocity of acoustic waves along the $\langle 011\rangle$ *crystallographic direction in a* (100) *silicon wafer (*c_{22} *= 165.7,* c_{33} *= 194.4,* c_{23} *= 63.9,* c_{44} *= 79.6 GPa).*

shown in the figure. It should be pointed out that those curves depend only on the properties of the material, and not on the geometry of the resonator.

Once $v(\xi)$ has been obtained, it is straightforward to relate it to the resonant frequencies of a resonator of given dimensions. By definition, $v = \omega / k_z$ and $k_z = 2\pi / \lambda_z$, and from these two equalities it follows that $f\lambda_z = v$. Moreover, at resonance λ_z must be an integer submultiple of $2W$, that is $\lambda_z = 2W/n_z$, hence

$$f = \frac{1}{\lambda_z} v(\xi) = \frac{n_z}{2W} v(n_z t_h / 2W) \tag{6}$$

Therefore the relationship between the resonator dimensions and its resonant frequencies can be obtained from $v(\xi)$ simply by changing the scales on the v and ξ axes.

ANSYS MODEL

To complement to the analytical model described in the previous section, we have also developed a SiBAR model for the ANSYS simulator that accounts for both the finite length of the resonator and the electromechanical transduction in the capacitive gaps, which is an integral part of the device behavior.

The orthotropic SOLID95 model is used for the resonating bar. Electromechanical transduction is modeled with two arrays of TRANS126 elements generated by the EMTGEN macro after the bar has been meshed. A number of resistors and capacitors model the test setup used for resonator testing and characterization [3]. The equivalent schematic diagram of the complete ANSYS model is shown in Figure 3: C_s and C_d model the gap capacitances, C_{ps} and C_{pd} the parasitic pad capacitances, and R_S and R_L the internal resistances of the test instruments.

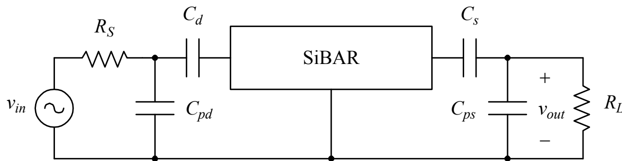

Figure 3: Equivalent circuit of the ANSYS model, including test setup.

Each simulation of the ANSYS model consists of a static analysis, which accounts for the effect of the DC polarization voltage, followed by a harmonic analysis. The simulation results include the values of all the node voltages, which makes it possible to generate plots of the voltage gain $A_v = v_{out} / v_{in}$ over the given range of frequencies, as shown in Figure 4. Many parameters related to the resonator performance can then be evaluated based on the location and magnitude of the peaks in the graph of $|A_v|$, including the effects of the resonator dimensions, the polarization voltage and the magnitude of the capacitive gaps not only on the resonant frequency, but also on the insertion loss.

The selection of the damping ratio used by ANSYS in its harmonic analysis (DMPRAT) merits some comment. The value of DMPRAT was chosen so that the simulated insertion loss of the resonator matched previously measured insertion losses of similar devices in the frequency range of interest. Consequently, this ANSYS model cannot provide reliable a-priori estimates of a resonator's insertion loss. On the other hand, once the value of DMPRAT has been selected in this way, the model can be expected to provide reasonably accurate information about how changes in the resonator dimensions affect the overall voltage gain A_v, provided that the resonant frequency does not change much. This is based on the assumption that the total rate of energy losses remains relatively constant within a relatively narrow frequency range.

To illustrate the model's capabilities, we present the results of the simulations of a set of SiBARs having the same length (400 μm) and width (40 μm), but varying thickness. The thickness values were chosen so that the main resonant peak would fall on the first dispersion curve of Figure 2. Figure 5 compares the values of the resonant frequency obtained from the ANSYS simulations with those predicted by the analytical model: it can be seen that the two models are in excellent agreement.

The plot of the simulated values of $|A_v|$ for the same set of SiBARs is shown in Figure 6. As can be seen in the figure, at first the magnitude of the voltage gain increases with the thickness of the device, because of the corresponding increase in the capacitive transduction area. Beyond a certain point, however, further increases in the thickness actually cause the voltage gain to decrease. This

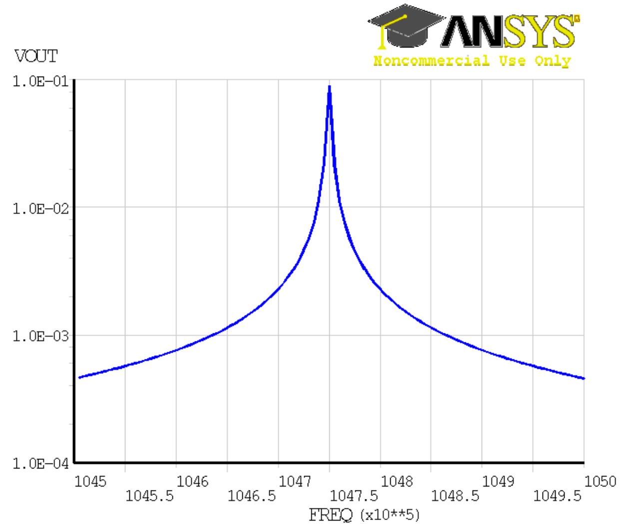

Figure 4: Simulated frequency response of a $400\mu m \times 40\mu m \times 20\mu m$ SiBAR.

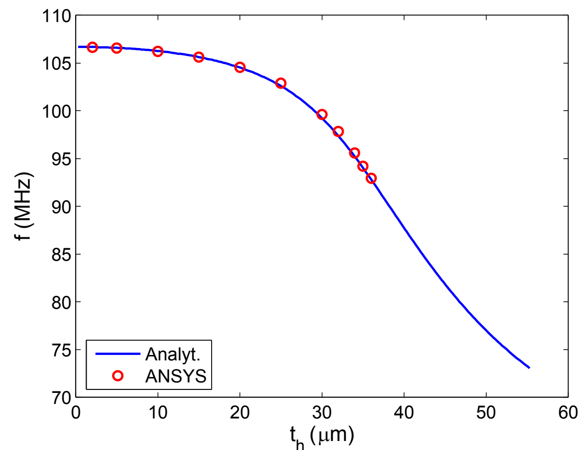

Figure 5: Resonant frequency vs. SiBAR thickness.

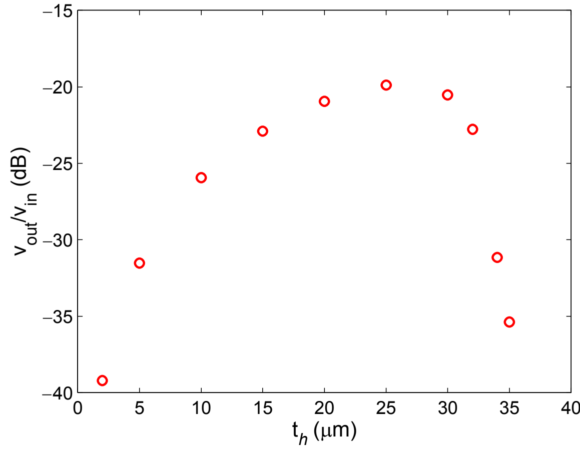

Figure 6: Plot of voltage gain vs. SiBAR thickness obtained from ANSYS simulations.

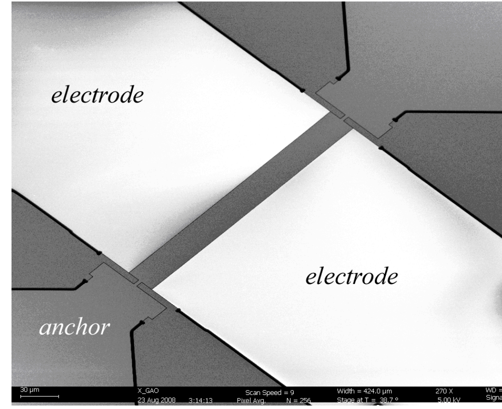

Figure 7: SEM view of a SiBAR fabricated in 10μm thick SOI with a capacitive gap of 300 nm.

phenomenon can be explained, at least in part, by a decrease in the efficiency of the electrostatic transduction in the capacitive gaps due to deterioration of the mode shape [5].

EXPERIMENTAL VERIFICATION

Both models were validated against measurements taken on SiBARs of various dimensions fabricated in 10 µm thick SOI. Device definition includes sub-micron trench formation using DRIE, followed by 3 µm wide peripheral trench etching, and HF release. A SEM micrograph of a sample device fabricated with this process is shown in Figure 7.

Table 1 compares the values of the resonant frequencies predicted by both models with those obtained from device measurements. The table shows also the relative error incurred when the approximate formula

$$f = \frac{n_z}{2W}\sqrt{\frac{E}{\rho}} \tag{7}$$

is used to estimate the resonant frequency of the SiBAR [3]. In all models, the value of W was set equal to the measured width of the device, so that the comparison would not be affected by process variations. In (7), the value of E was set to 169 GPa.

It is readily seen that the values of the resonant frequencies predicted by the models described in this paper are substantially more accurate than those given by (7), and that the error associated with the latter formula grows as the ratio $\xi = t_h/\lambda_z = n_z t_h/2W$ increases. This is consistent with the relationship between resonant frequency and SiBAR thickness predicted by both models (Figures 2 and 5), which show a gradual decrease in the resonant frequency of the device as its thickness increases.

CONCLUSIONS

For the first time, the models described in this paper make it possible to perform an accurate quantitative analysis of SiBARs, and to predict with a certain degree of confidence key parameters such as resonant frequency, frequency response and insertion loss. Both models can be effective aids in the design of high performance SiBARs.

ACKNOWLEDGEMENTS

This work was supported by DARPA under the Analog Spectral Processors program.

REFERENCES

[1] J. Wang, Z. Ren and C. T.-C. Nguyen, “Self-aligned 1.14 GHz vibrating radial-mode disk resonators,” in *Proc. TRANSDUCERS 2003*, vol. 2, pp. 947–950.

[2] S. Pourkamali, G.K. Ho and F. Ayazi, “Vertical capacitive SiBARs,” in *Proc. MEMS 2005*, pp. 211–214.

[3] S. Pourkamali, G. K. Ho and F. Ayazi, “Low-impedance VHF and UHF capacitive silicon bulk acoustic wave resonators – Parts I and II,” *IEEE Trans. Electron Devices*, vol. 54, no. 8, pp. 2017–2030, Aug. 2007.

[4] J. F. Rosenbaum, *Bulk Acoustic Wave Theory and Devices*, Artech House, Boston, 1988.

[5] G. K. Ho, “*Design and Characterization of Silicon Micromechanical Resonators*,” Ph. D. Thesis, Georgia Institute of Technology, 2008.

Table 1: Comparison with measured data

Length (μm)	Width (drawn) (μm)	Width (meas.) (μm)	Mode order (n_z)	Res. freq. (meas.) (MHz)	Analytical model		ANSYS model		Equation (7)	
					Freq. (MHz)	Error (%)	Freq. (MHz)	Error (%)	Freq. (MHz)	Error (%)
310	40	39.97	1	106.308	106.34	0.03	106.23	-0.07	106.5	0.18
			3	299.082	297.92	-0.40	297.85	-0.41	319.61	6.86
400	40	39.86	1	106.5	106.6	0.09	106.59	0.08	106.8	0.28
216	27	26.94	1	157.064	156.84	-0.14	156.86	-0.13	158.1	0.66
270	27	26.96	1	157.062	156.73	-0.21	156.74	-0.20	157.9	0.53
240	24	23.91	1	176.452	176.12	-0.19	176.17	-0.16	178.1	0.93
200	20	19.90	1	210.628	209.97	-0.31	210.06	-0.27	214	1.6